Brain Topogr (2007) 19:107–123
DOI 10.1007/s10548-007-0018-1

ORIGINAL PAPER

Estimate of Causality Between Independent Cortical Spatial Patterns During Movement Volition in Spinal Cord Injured Patients

Laura Astolfi · Hovagim Bakardjian · Febo Cincotti · Donatella Mattia · Maria Grazia Marciani · Fabrizio De Vico Fallani · Alfredo Colosimo · Serenella Salinari · Fumikazu Miwakeichi · Yoko Yamaguchi · Pablo Martinez · Andrzej Cichocki · Andrea Tocci · Fabio Babiloni

Accepted: 17 January 2007 / Published online: 19 June 2007

Abstract Static hemodynamic or neuroelectric images of brain regions activated during particular tasks do not convey the information of how these regions communicate to each other. Cortical connectivity estimation aims at describing these interactions as connectivity patterns which hold the direction and strength of the information flow between cortical areas. In this study, we attempted to estimate the causality between distributed cortical systems during a movement volition task in preparation for execution of simple movements by a group of normal healthy subjects and by a group of Spinal Cord Injured (SCI) patients. To estimate the causality between the spatial distributed patterns of cortical activity in the frequency domain, we applied a series of processing steps on the recorded EEG data. From the high-resolution EEG recordings we estimated the cortical waveforms for the regions of interest (ROIs), each representing a selected sensor group population. The solutions of the linear inverse problem returned a series of cortical waveforms for each ROI considered and for each trial analyzed. For each subject, the cortical waveforms were then subjected to Independent Component Analysis (ICA) pre-processing. The independent components obtained by the application of the ThinICA algorithm were further processed by a Partial Directed Coherence algorithm, in order to extract the causality between spatial cortical patterns of the estimated data. The source-target cortical dependencies found in the group of normal subjects were relatively similar in all frequency bands analyzed. For the normal subjects we observed a common source pattern in an ensemble of cortical areas including the right parietal and right lip primary motor areas and bilaterally the primary foot and posterior SMA areas. The target of this cortical network, in the Granger-sense of causality, was shown to be a smaller network composed mostly by the primary foot motor areas and the posterior SMA bilaterally. In the case of the SCI population, both the source and the target cortical patterns had larger sizes than in the normal population. The source cortical areas included always the primary foot and lip motor areas, often bilaterally. In addition, the right parietal area and the bilateral premotor area 6 were also involved. Again, the patterns remained substantially stable across the

H. Bakardjian · P. Martinez · A. Cichocki
Laboratory for Advanced Brain Signal Processing, Riken Brain Science Institute, Hirosawa, Wako, Saitama, Japan

L. Astolfi · F. Cincotti · D. Mattia · M. G. Marciani · F. De Vico Fallani · F. Babiloni
IRCCS ''Fondazione Santa Lucia'', Rome, Italy

F. Babiloni
Dipartimento di Fisiologia umana e Farmacologia, University of Rome ''La Sapienza'', Rome, Italy

F. De Vico Fallani · A. Colosimo
Centro di Ricerca de ''La Sapienza'' per l'Analisi dei Modelli e dell'Informazione nei Sistemi Biomedici, Rome, Italy

F. Miwakeichi
Laboratory for Dynamics of Emergent Intelligence, Riken Brain Science Institute, Hirosawa, Waka-shi, Saitama, Japan

Y. Yamaguchi
Department of Medical System Engineering, Faculty of Engineering, Chiba University, Chiba, Japan

L. Astolfi · S. Salinari · A. Tocci
Department of Informatica e Sistemistica, University of Rome ''La Sapienza'', Rome, Italy

F. Babiloni (✉)
Department of Human Physiology and Pharmacology, University of Rome ''La Sapienza'', P.le A. Moro 5, 00185 Rome, Italy
e-mail: Fabio.Babiloni@uniroma1.it

different frequency bands analyzed. The target cortical patterns observed in the SCI population had larger extensions when compared to the normal ones, since in most cases they involved the bilateral activation of the primary foot movement areas as well as the SMA, the primary lip areas and the parietal cortical areas.

Keywords ThinICA · Distributed current density estimates · Brodmann areas · Inverse problem · High-resolution EEG · Functional connectivity · Partial Directed Coherence

Introduction

Nowadays, different non-invasive brain imaging techniques are able to provide images of the human cortical activity, based on hemodynamic (functional Magnetic Resonance Imaging, fMRI), metabolic (Positron Emission Tomography, PET) or electromagnetic (Electroencephalography, EEG and Magnetoencephalography, MEG) measurements. However, static images of brain regions activated during particular tasks do not convey the information of how these regions communicate with each other. In fact, the concept of brain connectivity is viewed as central for the understanding of the organized behaviour of cortical regions beyond the simple mapping of their activity [20, 33, 38]. This organization is thought to be based on the interaction between different and differently specialized cortical sites. Cortical connectivity estimation aims at describing these interactions as connectivity patterns which reflect the direction and strength of the information flow between cortical areas. To achieve this, several methods have been already applied on data gathered using both hemodynamic and electromagnetic techniques [13–15, 25, 51, 53]. Two main definitions of brain connectivity have been proposed over these years: functional and effective connectivity [23]. While functional connectivity is defined as temporal correlation between spatially remote neurophysiologic events, the effective connectivity is defined as the simplest brain circuit, which would produce the same temporal relationship as observed experimentally between cortical sites. As for the functional connectivity, the several computational methods proposed to estimate how different brain areas are working together typically involve the estimation of some covariance properties between the different time series measured from the different spatial sites during motor and cognitive tasks studied by EEG and fMRI techniques [24, 25, 35, 53]. So far, the estimation of functional connectivity on EEG signals has been addressed by applying either linear and non-linear methods which can both disclose the direct flow of information between scalp electrodes in the time domain, although with different computational demands [17, 34, 41, 47, 49, 50, 52]. In addition, due to the evidence that important information in the EEG signals are often coded in the frequency rather than time domain (reviewed in [43]) attention has been focused on detecting frequency-specific interactions in EEG or MEG signals by analyzing the coherence between the activity of pairs of structures [40]. Coherence analysis does not have, however, a directional nature (i.e., it just examines whether a link exists between two neural structures, by describing instances when they are in synchronous activity), and it does not provide directly the direction of the information flow. In this respect, two multivariate spectral techniques called Directed Transfer Function (DTF) and Partial Directed Coherence (PDC) were proposed [11, 36] to determine the directional influences between any given pair of channels in a multivariate data set. These estimators are able to characterize at the same time the direction and the spectral properties of the brain signals, requiring only one multivariate autoregressive (MVAR) model to be estimated from all the EEG channel recordings. The DTF and PDC techniques have been demonstrated [10, 36] to rely on the key concept of Granger causality between time series [26], according to which an observed time series $x(n)$ causes another series $y(n)$ if the knowledge of $x(n)$'s past significantly improves prediction of $y(n)$; this relation between time series is not reciprocal, i.e., $x(n)$ may cause $y(n)$ without $y(n)$ necessarily causing $x(n)$. This lack of reciprocity allows the evaluation of the direction of information flow between structures.

So far, the causality between brain signals have been assessed by using time varying information derived from hemodynamic or electromagnetic signals recorded at the scalp level [36] or estimated at the cortical level [2, 3, 8]. However, the causality estimation from these brain functional waveforms can depict a single pattern of connectivity involving several brain areas, for each time segment or in every frequency band analyzed. Since it is well known that the brain does not produce any ''single waveform'' but rather engages several distributed cortical areas in order to process information, a question arose about the appropriateness of the estimation of the functional connectivity between waveforms. In particular, the question is whether, instead of estimating the causality between single waveforms derived from the different cortical or scalp areas, it is possible estimate the causality between ''spatial patterns of brain cortical activations''. In fact, it is reasonable to pose the question if it could be more interesting to estimate the causality (in the sense of the Granger definition) between the activation of distributed cortical systems or just observe the causality between isolated waveforms.

In this report, we attempted to estimate the causality between distributed cortical systems during the execution

and the imagination of simple movements in a group of normal healthy subjects and in a group of Spinal Cord Injured patients (SCI). To estimate the causality between the spatial distributed patterns of cortical activity in the frequency domains, we applied a series of processing steps on the recorded EEG data. First, we estimated the cortical activity from the EEG recordings by using realistic head and cortical models for each subjects. This was obtained by considering the cortical activity occurring in the Brodmann areas used to segment the cortical models used. The cortical activities were estimated by using the solutions of the EEG linear inverse problems as described previously [2, 3, 8]. Furthermore, we applied Independent Component Analysis (ICA) pre-processing on the cortical waveforms derived from the Brodmann areas for each subject. The application of the ICA to the cortical waveforms derived from the Brodmann areas returned a series of basic spatial patterns of activations as well as the temporal variation of these patterns along the estimated cortical waveforms. The key point of this processing is the estimation of causality between the temporal independent components calculated for the cortical data by using the PDC [11]. The application of the PDC between two different independent components estimated from the computed cortical waveforms returned an estimation of the causality between couples of distributed cortical activation patterns. Hence, the causality of the activation of the distributed cortical areas occurred not at the level of single waveforms, but rather at the level of a coordinated series of cortical areas, as described by the spatial independent components obtained by the ICA.

In this study, we propose to estimate the causality of the cortical connectivity patterns by exploiting the combined use of ICA and PDC techniques applied to high-resolution EEG signals which exhibit a higher spatial resolution than conventional cerebral electromagnetic measurements made over or outside of the scalp. The high-resolution EEG technique includes the use of a large number of scalp electrodes, realistic models of the head derived from structural magnetic resonance images (MRIs), and advanced processing methodologies related to the solution of the linear inverse problem. These methodologies allow the estimation of cortical current density from sensor measurements [7, 27, 32, 42]. Subsequently, a novel combination of ICA and PDC methods was applied to the cortical estimates obtained from high-resolution EEG data related to a movement volition task in SCI patients and in a control group of normal healthy subjects. The questions at the basis of this paper are the following:

1. Do there exist different cortical networks elicited by the proposed volitional tasks causing (in the Granger sense) the activity of other cortical networks?
2. Are there specific frequency bands in which such causality relations between the cortical networks are maximally present during the investigated task?
3. Are there significant differences in the cortical networks between normal subjects and SCI patients elicited for the investigated task? Are these differences (if any) related to any particular frequency bands?

Methods

The estimation of the cortical activity from high-resolution EEG recordings

High-resolution EEG recordings

Six right-handed healthy subjects and five patients with a spinal cord injury (SCI) participated in the study. The SCI was of traumatic aetiology and located at the cervical level (C7) and all the patients had not suffered from a head or brain lesion associated with the trauma leading to the injury. The SCI patients were unable to move their upper and lower limbs. For the electroencephalographic (EEG) data acquisition, subjects were comfortably seated on a reclining chair, in an electrically shielded, dimly lit room. Informed consent was obtained from each subject after explanation of the study, which was approved by the local institutional ethics committee. In the present event-related experimental design, we adopted a simple motor task consisting of repetitive self-generated overt movement executions (for control subjects) and attempts for executions (for SCI patients) of the right foot dorsal flexion at the ankle, simultaneously with the lips pursued by the subjects in both groups (the SCI patients were able to move their lips). The absence of external cues was chosen in order to avoid that any part of the observed EEG task-induced activities related to sensory perception or to processing of pacing stimuli *per se*. A 58-channel EEG system (BrainAmp, Brainproducts GmbH, Germany) was used to record the brain electrical potentials by means of an electrode cap with sensors placed according to the extended 10–20 international system. Structural MRIs of the subject's head were taken with a Siemens 1.5T Vision Magnetom MR system (Germany). The EEG was sampled at 200 Hz, and 100 trials of 8-s durations were recorded for each subject. Figure 1 shows the electrode cap used for the EEG recordings and a particular head model employed for the computations in a normal subject. The figure presents the four steps involved in the generation of the lead field matrix for the estimation of the cortical current density from high-resolution EEG recordings, starting from the MRI images, the EEG electrode cap, and through the generation

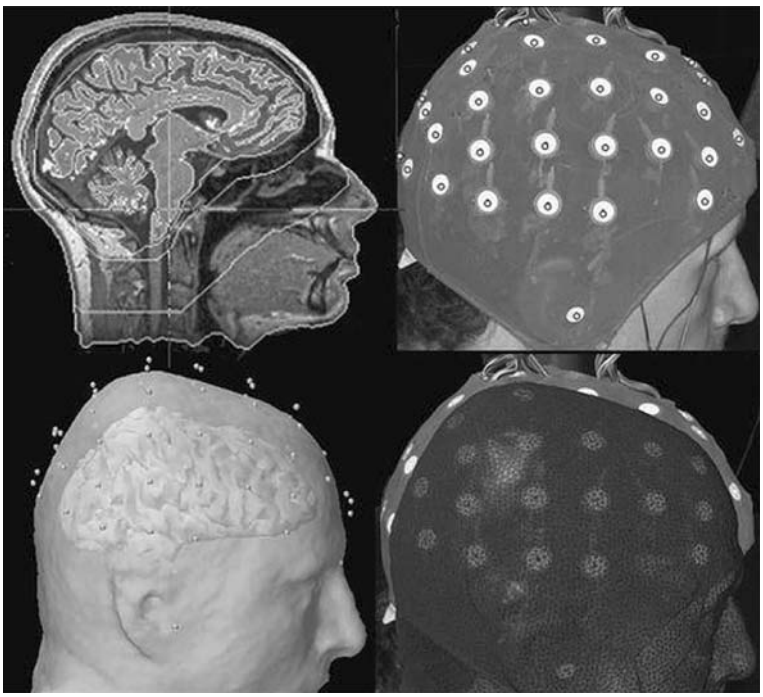

Fig. 1 Four steps involved in the generation of the lead field matrix for the estimation of cortical current density from high resolution EEG recordings. From left to right, from top to the bottom the MRI images are shown for a healthy subject, the generation of the model of the head and the superposition with the electrodes cap

of the model of the head and its final superposition with the electrodes cap.

Applying the tools for the estimation of the cortical activity and connectivity

(1) We estimated the cortical activity from the high-resolution EEG recordings, by using realistic head models and a cortical surface model with an average of 5000 dipoles, which were uniformly distributed (see Appendix). The estimation was obtained by the application of a linear inverse procedure [8, 27]. Cortical activity was then estimated in regions of interest (ROIs) generated by the segmentation of the Brodmann areas (B.A.) on the accurate cortical model used. Bilateral ROIs considered in this analysis were: the primary motor areas for the foot (MIF) and for the lip movement (A4_Lip), the posterior supplementary motor areas (SMAp), the standard premotor areas (A6), the posterior parietal areas (A7) and the cingulate motor areas (CMA). The labels of the cortical areas contain also a postfix characterizing the considered hemisphere (R, right, L, left). Such ROIs were segmented on the basis of Talairach coordinates and anatomical landmarks available. ROIs representing the supplementary motor area (SMA) were obtained from cortical voxels belonging to the more general BA 6. In particular, the posterior SMAp was depicted bilaterally on the medial frontal wall by following the anatomical landmarks recommended by Picard and Strick [44]: the anterior border of the SMAp corresponded to a plane perpendicular to the anterior–posterior commissure (AC-PC) line at the level of the AC (VAC), and a perpendicular plane at the level of the posterior commissure (VPC) represented the SMAp posterior border. Figure 2 presents the cortical areas as obtained for the realistic head models generated for each healthy subject. It is possible to note the different positions of the same cortical areas on the cerebral surface between the subjects.
For each time point of the recorded EEG we solved the linear inverse problem, estimated the magnitude for each one of the thousands of dipoles used for cortical modelling. Then, we computed the average of the magnitudes of such dipoles in each ROI considered, for each time point considered. The resulting cortical waveforms, one for each predefined ROI, were then subjected to the ICA analysis to reveal their independent components. Since the cortical waveforms were obtained for each single trial and recorded for each experimental subject, the single-trial signals were concatenated to each other, after detrending, for consecutive analysis as described in details further below.

The estimation of distinct cortical activity patterns by using independent component analysis (ICA)

As described above and in the Appendix, the estimation of the cortical activity from the EEG recordings returns a cortical current density waveform for each ROI considered, in each trial analysed. However, it was advantageous to study

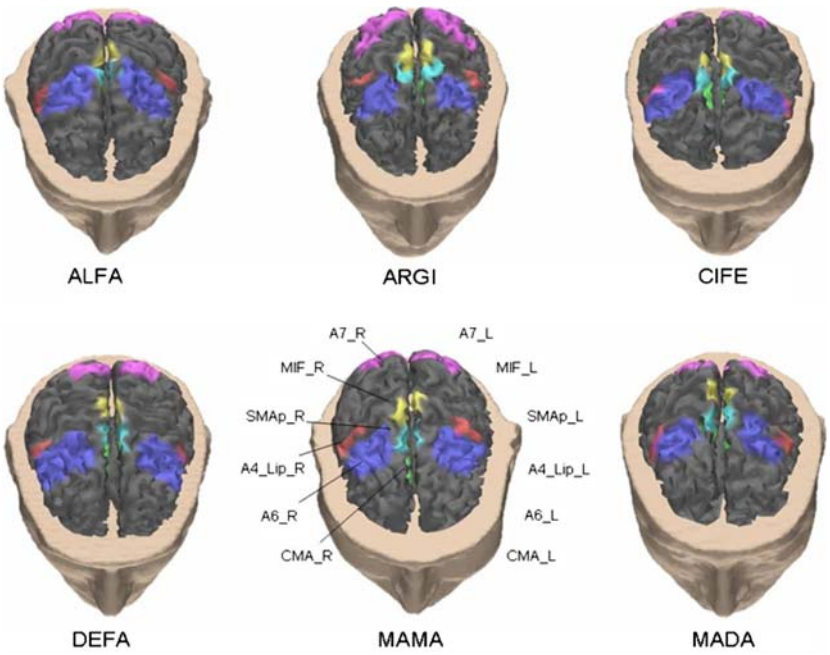

Fig. 2 The cortical regions of interest (ROIs) employed in this study for the normal population investigated. Each ROI is represented with a different colour, and the used colour scheme is common across the different subjects. Note that the Cyngulate Motor Areas, located in the mesial central part of the cortical surface, are hidden in the interhemispheric scissure

further these spatially distributed cortical activities in the ROIs by separating them into independent components each of which could be projected back to a distinct spatial pattern.

In order to apply the ICA to the cortical current density waveforms, the following steps have been applied:

(2) Each trial was segmented in order to extract a data section related to the preparation of the movement to be performed, starting at 1.5 s before the electromyographic (EMG) onset. The resulting *j*th trial will be denoted as $\mathbf{X}_j$, where $\mathbf{X}_j$ is the matrix composed by the number of ROIs times the number of samples for the *j*th trial, where $j = 1...100$ (total number of trials).
(3) The mean value of each $\mathbf{X}_j$ matrix was removed. The resulting matrix will be denoted as $\overline{\mathbf{X}}_j$.
(4) Each trial was concatenated to the next one, and a matrix $\mathbf{X}$ has been obtained composed by the number of rows, equal to the number of ROIs, and the number of columns, equal to the number of samples in each trial, times the number of trials considered. In a concise form, we have $\mathbf{X} = [\overline{\mathbf{X}_1}, \overline{\mathbf{X}_2}, \ldots, \overline{\mathbf{X}_{100}}]$;
(5) The mean value of the $\mathbf{X}$ matrix was removed and the resulting matrix was filtered with a zero-delay low-pass FIR filter at 40 Hz.
(6) An ICA [16] algorithm was applied to the $\mathbf{X}$ matrix, in order to obtain the demixing matrix $\mathbf{W}$ and the matrix of the independent components Y, according to the following equation [16]:

$$\mathbf{Y} = \mathbf{W}\mathbf{X} \tag{1}$$

In agreement with the notation described above, it is also possible to compute the inverse relation from the array of the independent component Y to the original concatenated current density waveforms $\mathbf{X}$ by using the mixing matrix $\mathbf{A}$ which is the pseudo-inverse of the matrix $\mathbf{W}$ according to the equation:

$$\mathbf{X} = \mathbf{A}\mathbf{Y} = \mathbf{W}^{+}\mathbf{Y} \tag{2}$$

The matrix $\mathbf{A}$ is the matrix of the spatial patterns (in the cortical space) which when multiplied by the time-varying loads of all independent components Y, returns the original data by back-projection. Specifically, in this study we used the ThinICA algorithm [12, 18, 19], which allowed a mixed 2nd and 4th order cumulants for ICA, and based on criteria that jointly performed the maximization of higher-order cumulants and second-order time-delay covariance matrices. Such approach allows us to estimate optimally sources which have temporal structures and they modeled as autoregressive processes (AR), as well as independent identical distributed non-Gaussian components. The employed simultaneous ICA extraction, which used thin (economy size) SVD factorizations, combined the robustness of the joint approximate diagonalization techniques with the flexibility of the methods for blind signal extraction.

(7). In order to deal with an $\mathbf{A}$ matrix having normalized values, it is possible to transfer the differences in intensity from the $\mathbf{A}$ matrix to the $\mathbf{Y}$ component, through dividing each *i*th column of the $\mathbf{A}$ matrix by its own maximum value and also multiplying the *i*th component of the $\mathbf{Y}$ matrix by the same value. This procedure was performed and returned a normalized $\mathbf{A}$ matrix, which

we'll call $\mathbf{A}^{norm}$, as well as a new independent component matrix **Y,** with its values rescaled according to such maxima, which we'll call $\mathbf{Y}^{scal}$. Note that it is still true that

$$\mathbf{X} = \mathbf{A}^{norm}\ \mathbf{Y}^{scal} \quad (3)$$

The procedure, as detailed above, returned an estimate of the $\mathbf{A}^{norm}$ matrix that described the mixing of the independent spatial cortical activations for the gathered data, as well as a component matrix $\mathbf{Y}^{scal}$ revealing the temporal behaviour of these independent activations. Hence, each *i*th component of the $\mathbf{Y}^{scal}$ matrix was related to the time-varying presence of the *i*th spatial pattern described by the *i*th column of the $\mathbf{A}^{norm}$ matrix in the gathered EEG data as represented by the **X** matrix. Now, in order to assess the possible causality relations between the cortical pattern activations, we estimated the connectivity values between the different independent components described by the matrix $\mathbf{Y}^{scal}$. The connectivity values were obtained by using the PDC algorithm.

The estimation of the causality between the cortical activity patterns by using Partial Directed Coherence (PDC)

(8) The Partial Directed Coherence (PDC; [10]) algorithm, was applied to the $\mathbf{Y}^{scal}$ component matrix and returned a series of causality relationships between the different independent components, each one related to a particular spatial activity distribution. The causality patterns between the independent components were considered further in this analysis only if they were statistically significant, in agreement with the procedure already described previously [2, 3]. A statistical connection between the *i*th and the *j*th components of the $\mathbf{Y}^{scal}$ matrix (represented as Yi –> Yj) means that the series of cortical ROIs involved in the *i*th spatial pattern of the $\mathbf{A}^{norm}$ matrix will cause an activity in the series of cortical ROIs involved in the *j*th spatial pattern of the same matrix $\mathbf{A}^{norm}$. In the sense of the Granger theory, the inclusion of the Yi independent component (with a distinct pattern of cortical areas corresponding to the *i*th independent component) improves the predictions of the time series of the Yj independent components in the multivariate autoregressive model.

(9) For each subject analyzed, three frequency bands were investigated (theta (4–7 Hz), alpha (8–12 Hz) and beta (12–30 Hz)). Only causal links with the highest connectivity in each band were used for successive analysis. Such connectivity links were those with the highest statistical significance with respect to the random values of the PDC computed by using a shuffling procedure [3, 8, 36]. A statistical difference threshold of $p < 0.01$ was adopted for all the computations presented here, including the comparisons with the shuffled-phase signals. Hence, for each frequency band and for every subject, we identified a series of four most-connected components corresponding to cortical spatial patterns ('sources') that ''caused'' or drove other cortical spatial patterns ('targets') during the execution of a task. In this study, these source-target patterns were related to the preparation of the motor task for 1.5 s before its onset.

Since the independent components were not ordered between subjects, a possible problem arose when a comparison of these spatial patterns between the subjects has to be performed, in order to extract inferences related to the group behaviour. In fact, it is well known that the numbering of the spatial components is not consistent between different subjects, i.e., the component number 4 for the subject *k*th may not be the same as the component number 4 for the subject *j*th, and so forth. Then, it is interesting to have a tool able to couple the independent components between subjects on the basis of their spatial patterns. This is important since the goal is to build a set of couples of cortical spatial patterns (one that ''drives'' and the other that is driven) that are common for all the investigated populations. In order to obtain such ''average'' cortical pattern a series of operations have to be performed. The approach pursued in this study can be described in the following way:

(10) Each of the top four selected cortical component couples for each subject of the healthy and SCI study groups was back-projected to the cortical ROI space.

(11) The state of each reconstructed ROI corresponding to this single component was evaluated by a binary representation, containing 1s or 0s, to mark whether the cortical area was activated or not activated by the component. Specifically, the 1s indicated that the normalized dipolar cortical activation exceeded the threshold interval (–0.2:0.2).

(12) For each subject, the source-target causality binary representation for each of the four most-connected couples, as described above, was compared with all the other top couples of activation representations for all the other subjects analyzed. Such comparisons were performed by using a Pearson correlation index. Each comparison was made taking into account the distribution of the cortical areas in patterns that ''caused'' another one and the distribution of the areas in cortical patterns that were ''caused'' by the previous one.

(13) The correlation indices between all couples of binary representations between the subjects were then used to compile a ranking list of pattern similarities. The

top-matching couples of representations for each subject were selected to form a final list from which the average was computed and represented the coupling between the patterns. This average measure characterized the causality links between the spatial cortical patterns in the population.

(14) For each spatial source or target pattern, the representations of some cortical ROIs in the presented Figs. 3–8 contain spheres, indicating the number of subjects in which these particular cortical ROIs are activated in the analyzed pattern. The higher the number of subjects in the population that have activated the *j*th ROI, the larger is the radius of the sphere for such ROI in the ''average'' representation. The colour of the spheres also codes the existence of the common activated ROI in the group of subjects considered. In particular, the yellow spheres show the presence of the activated ROI in all of the subjects belonging to the analyzed group, and such colour is associated with the greatest sphere size. The red colour is used to code the presence of the activated ROI in all but one subjects belonging to the group, and the size of the sphere is smaller than for the yellow one. The blue colour is used to code the presence of the activated ROI in all but two subjects, and the relative size is smaller than for the red one. If the activated ROI is present in all, but three subjects of the experimental group or less, then no sphere is drawn.

Following these procedures, it is possible to obtain different average'' couples of spatial patterns for each frequency band. Such ''average'' cortical patterns correspond to the time period of preparation for movement in the subjects.

Results

Following the methodology presented above, we estimated from the high-resolution EEG recordings the cortical waveforms at the ROIs selected for all the group population. The solution of the linear inverse problem returned a series of cortical waveforms for all ROIs considered and for all trials analyzed. In each subject, the cortical waveforms were then subjected to a ThinICA processing, according to the procedures depicted in the ''Methods'' section. The independent components obtained by the application of the ThinICA algorithms were then processed by the PDC algorithm, in order to extract the directed causality between the spatial cortical patterns of the

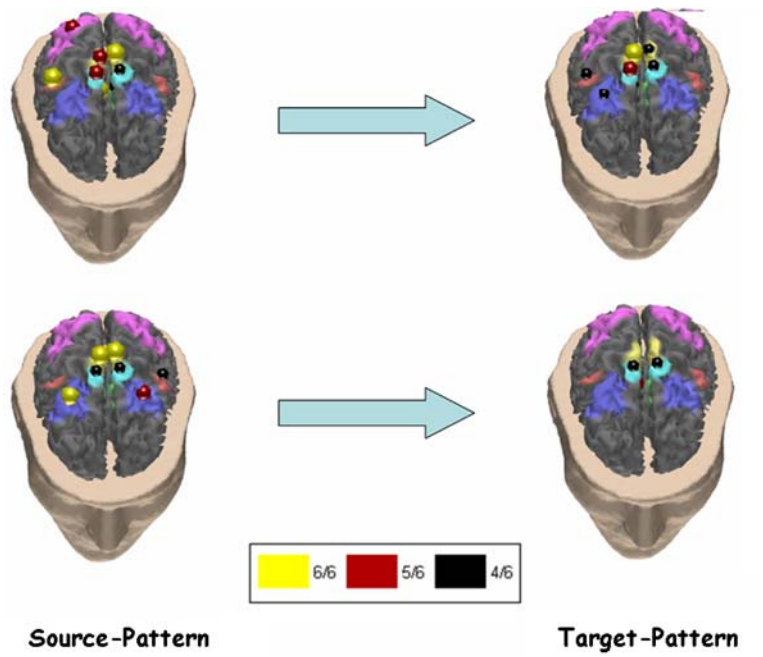

Fig. 3 Average cortical causality pattern in the theta band for the group of control subjects. Same conventions used in the previous figure. First row presents correlation patterns between the subjects with a value of 79.9%. Second row presents correlation patterns with values of 72%. The realistic head below shows the equivalent representations on the cortical surface. The colour of the spheres codes for the number of subjects in which the ROI is present in the spatial pattern. In yellow, the ROIs present in all the six subjects, in red the ROIs present in five subjects out of six and in black the ROIs present in four subjects. Note that the red sphere in the right cyngulate area in the target cortical pattern (on the right) is almost completely hidden from the cortical surface in the realistic reconstruction of the cortex presented here

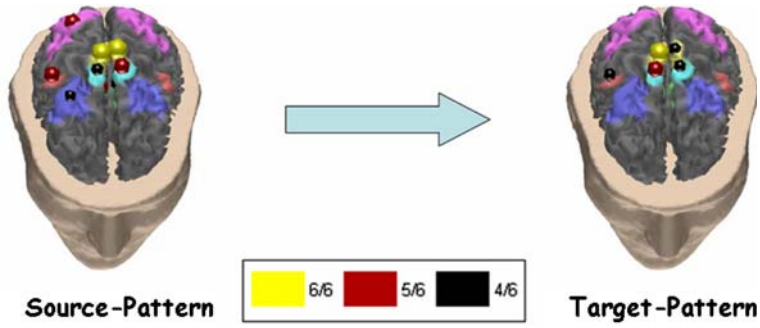

Fig. 4 The coupling patterns in the alpha frequency band for the group of normal subjects. Correlation index equal to 79%. Same conventions of the previous figure

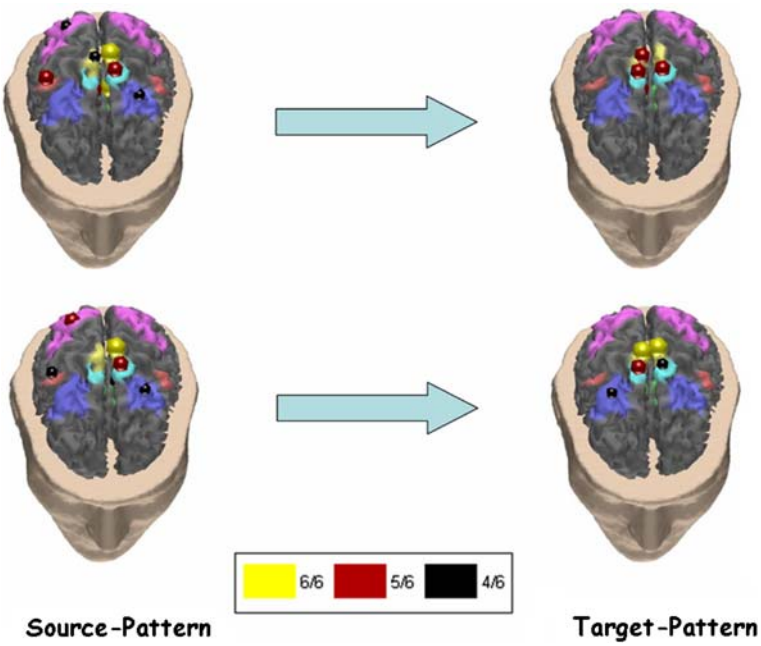

Fig.5 Causality patterns revealed in the normal subject population in the beta frequency band. First row: correlation index at 71%. Second row: correlation index at 72%. Same conventions are used as in the previous figure

estimated data. Such couples of cortical patterns were obtained for each one of the three frequency bands employed in this study. Note that the intensity of the spatial pattern of each square belongs to the interval (–1, 1), being normalized with the amplitude values moved into the temporal waveforms of the independent components (from the *j*th column of the $\mathbf{A}^{\text{norm}}$ matrix to the *j*th component of the $\mathbf{Y}^{\text{scal}}$ matrix).

We applied an appropriate algorithm to locate the similarities between the computed couples of cortical patterns in the different subjects, and the ''average'' couples of spatial patterns in each frequency band were then generated. The following figures illustrate these ''average'' causality patterns due to the preparation of an active foot movement in the different frequency bands analyzed for the group of normal subjects and to the volition of movement for the group of SCI subjects. As already described in the method section, here the yellow spheres indicate that all the subjects in the group have the same ROI engaged in the causality link between cortical patterns, while the red spheres on a ROI indicate that all the subjects but one have the same ROI activated, and the black spheres illustrate that all the subjects but two have the same ROI activated. In the following, only results from cortical causality patterns that presented a spatial correlation of more than 70% are displayed in the different frequency bands.

Normal population

Figure 3 shows the cortical pattern in the theta frequency band for the normal population analyzed.

Taking into consideration the yellow and the red spheres (6/6 or 5/6 subjects), it seems that in the theta frequency band there was a drive from a cortical network involving the right cingulate motor area (CMA), right foot movement area (MIF), as well as the right parietal area (A7) and supplementary motor area (SMA) toward the right MIF and SMA. In this pattern, the MIF bilaterally as well as the right premotor area (A6) was driving the right CMA. No other cortical coupling patterns were statistically

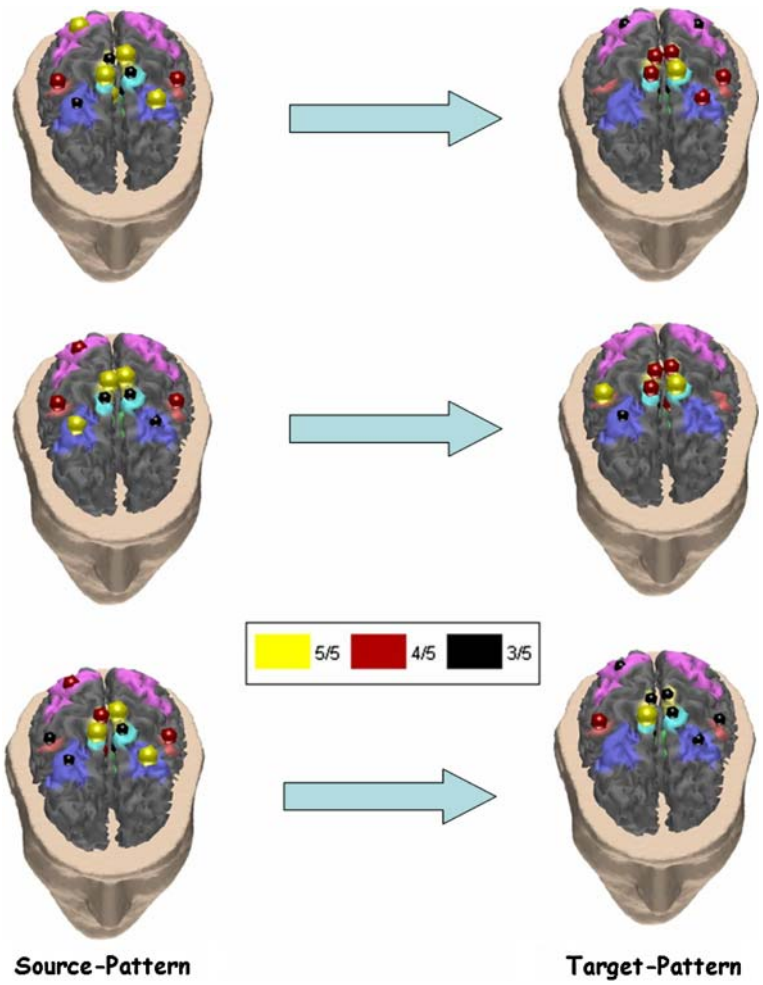

Fig. 6 Cortical causality pattern for the theta band in the SCI population. Correlation value between the population is 76.7% (first row). In the second row the correlation value is 77.6%, while in the third row the correlation is 74.6%. Same conventions than in the previous figures

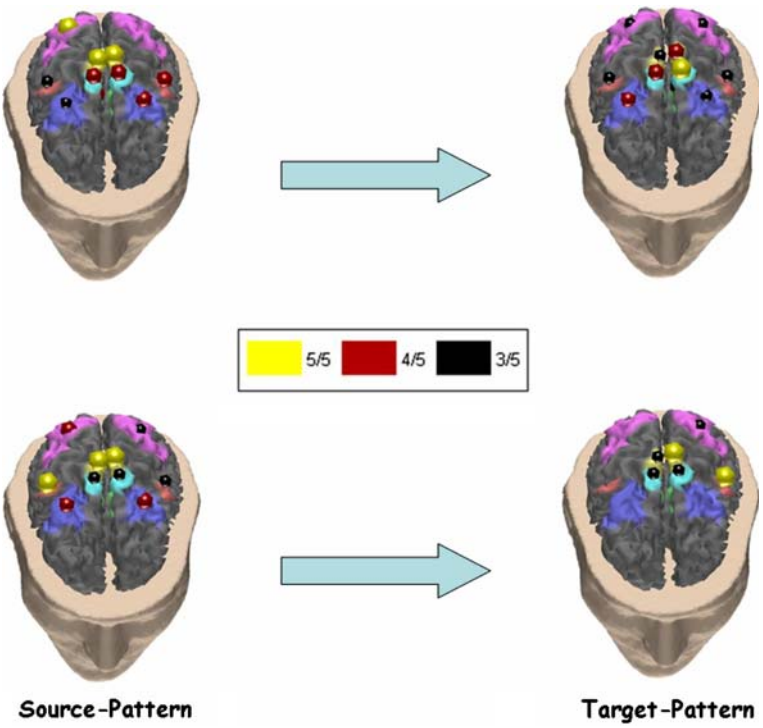

Fig. 7 Causality patterns presented in the SCI population in the alpha frequency band. First row shows a correlation index of 80%. Second row shows a correlation index of 73.8%

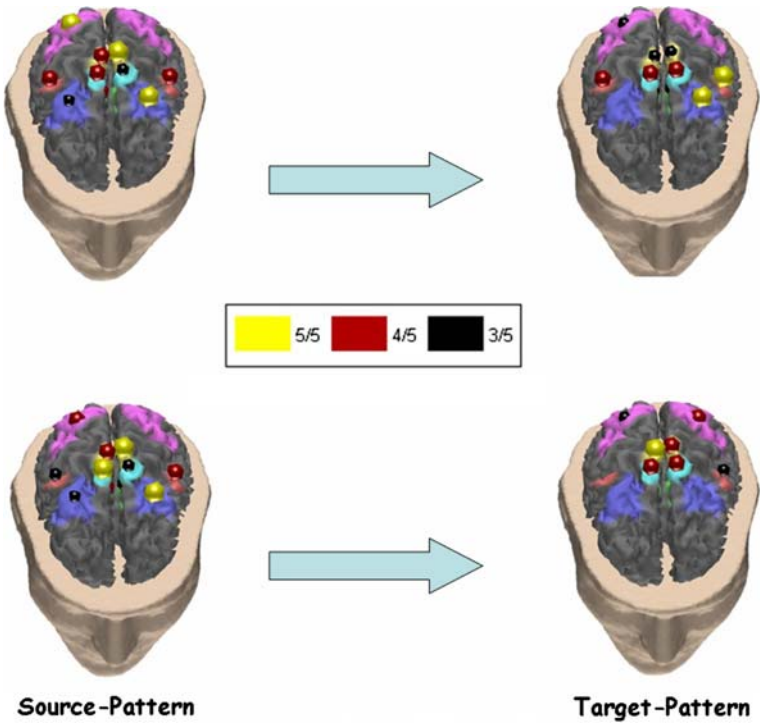

Fig. 8 Causality pattern presented in the SCI population in the beta frequency band. First row shows a correlation index of 79.4%, while the second row shows a correlation index of 71.4%

significant among the subjects analyzed with more than 70% correlation index in the theta frequency band.

The coupling patterns in the alpha frequency band for the group of normal subjects showed a correlation index equal to 79%. The pattern is presented in Fig. 4.

This pattern revealed that the activation of the primary motor area of the foot bilaterally (MIF), with contributions from the right parietal areas (A7) and CMA, was driving the right MIF and the SMA cortical areas.

We observed two cortical causality patterns over the 70% threshold of the correlation index in the beta frequency bands for the normal subjects in this study. In Fig. 5, the first row shows the causality pattern which had a correlation index of 71%, while the second row shows the causality pattern having a correlation index of 72%.

Such a pattern suggests a major involvement of the primary left foot area and the CMA in the driving of SMA, bilaterally. The second pattern available for normal subjects in the beta band is characterized by a slightly higher correlation index than before, which means a good agreement between the subjects. This second causality pattern in the normal group suggests that the primary left foot motor area was driving the activity in the primary motor areas bilaterally.

SCI population

The SCI population shows in this frequency band three spatial pattern with a correlation values more than 70%. They are presented in Fig. 6

The cortical causality patterns depicted above in the first two rows show a involvement of a large network of cortical areas on the left (yellow spheres) toward the activation of the left SMA (yellow sphere of the right panel). The second row presents a cortical causality pattern for the theta band different than those presented above. In such row the SCI group presents here a correlation index of 77.6% and the activation of the primary motor foot area that drives the activation of roughly the same areas plus the SMA bilaterally. The last causality pattern in the theta band over the 70% of the correlation index for the SCI subjects is presented in the third row. In this case, the pattern depicts the activation of a large network of cortical areas toward the right SMA.

In the alpha band the SCI population presents two spatial cortical patterns over the 70% of the correlation index, with values of correlation of 80% and 73.8%. The first pattern in the alpha band for the SCI population is presented in the first row of Fig. 7.

Such pattern suggests an involvement of the primary motor area of the foot area bilaterally as well as the parietal area driving the left SMA. The second cortical connectivity pattern in the alpha frequency band for the SCI group has a correlation index of 73.8% and it is presented in the second row of the previous figure. Such pattern is characterized by an involvement of the primary motor foot area and the area 4 right that drives the left motor areas (area 4 and MIF).

In the beta band, the SCI population presents two patterns of cortical causality having the correlation index over the 70%. In particular, the first row is presented in the first

row of Fig. 8 and has a correlation index of 79.4%. This correlation index is very high when compared to the highest index (72%) of the normal population.

This cortical pattern suggests an involvement of the left primary foot, SMA and A4 cortical areas as well as the right parietal areas (A7) that drives the cortical areas A4 and the SMA. The presence of the A7 is of interest in this driving pattern, when compared to the normal one. The second pattern for the SCI population has a correlation index of 71.4% and is presented in the second row of Fig. 8. This pattern is characterized by an activation of cortical areas similar to those activated before (bilateral primary foot area, A6) plus the right SMA and A7 that drives essentially the right primary foot area bilaterally as well as the ROIs representing the SMA.

Methodological considerations

The methodological approach presented here aims at describing the generation of a set of mathematical tools able to depict the existence of distributed cortical networks that drive, or ''cause'', in the sense of Granger theory, the activity of other distributed cortical networks, as revealed by analysis of data from high-resolution EEG recordings in humans. This methodological approach uses high-resolution techniques for the estimation of the cortical activity in regions of interest from EEG recordings. By using this technology we were able to estimate the cortical current density in particular ROIs depicted on the realistic model of the cortex and based on the Brodmann cortical areas for each subject. The precise description of each ROI was made possible by the use of realistic models of the cortex of each subject. Subsequently, the application of ThinICA algorithms for the estimation of independent cortical activations in the ROIs returned a set of time varying waveforms (temporal independent components) as well as a series of spatial patterns of activations (spatial independent components) that could be further processed. In particular, we analyzed the causal relationship between the independent components in the time domain, by using the established algorithms for the estimation of functional connectivity such as the DTF or PDC to unveil the causality between the ThinICA waveforms. In this way, it was possible to observe patterns of distributed cortical sources that ''caused'', in the sense of the Granger theory, other patterns of distributed cortical sources in different frequency bands. This means that the inclusion of a particular set of waveforms from the ''driving'' cortical patterns improved the prediction of the ''driven'' cortical patterns in the multivariate autoregressive modeling. The presented approach describes how cortical patterns could drive other cortical patterns, by using the concept that such patterns are ''independent'' in the sense provided by the application of an ICA to the cortical current density estimations. Specifically, the ThinICA method [12, 18, 19] was used in order to extract information about the cortical connectivity. In a previous similar approach, Miwakeichi and co-workers [39] demonstrated the decomposition into space time-frequency components of EEG signals obtained during cognitive tasks by using an analysis method called parallel factor analysis (PARAFAC).

The present study examined the performance of techniques commonly used to assess information flows between scalp electrodes and local field potentials [11, 36, 37] on real cortical waveforms obtained via the linear inverse problem solution, using the realistic head volume conductor models and high-density EEG recordings. The spatial resolution provided by the techniques presented here has been previously characterized in a series of simulation studies using the present ROI analysis approach [5–7, 9]. The connectivity estimator used in the present study is based on the Granger theory and MVAR models. The PDC technique has the advantage of providing connectivity links that can be interpreted in the sense of Granger causality, which includes a concept of directionality. Other techniques have been presented in the literature for the evaluation of functional connectivity of EEG/MEG data. For instance, the technique called Dynamic Imaging of Coherent Sources (DICS) [28, 29], which uses a spatial filter and a realistic head model, has been recently introduced and employed to assess connectivity between cortical areas from MEG data [28, 29, 45, 46]. This technique has the advantage, when compared to the PDC method used here, of a direct mathematical characterization of its spatial resolution of the point spread function [29]. However, spectral coherence or DICS techniques do not return directly the direction of the flow between cortical areas, though in the latter case DICS could be coupled with another technique able to estimate such directional flow, like the Directionality Index [48].

Application on normal and SCI patients of combined ICA and PDC techniques

In the normal population considered, the source patterns include bilaterally the primary foot areas as well as the posterior SMA (SMAp), while the involvement of the right primary lip motor areas and the posterior parietal areas is also noted. Such source cortical patterns are active across all the frequency bands analyzed. Always in the normal population, the target patterns across all the frequency bands considered are limited to the cortical networks involving the primary foot movement area and the posterior SMA bilaterally. Occasionally, the right primary motor area for the lip movement is also involved. No involvement of the parietal areas where observed as a

target of the cortical networks that acts as source patterns described above.

In summary, the source-target cortical patterns depicted in a group of normal subjects seems independent from the frequency bands analyzed and present as a source common pattern an ensemble of cortical areas including the right parietal and right lip primary motor areas and bilaterally the primary foot and posterior SMA areas. The target of this cortical network, in the Granger-sense of causality, is a network again composed by the foot primary motor areas and the posterior SMA bilaterally. A simple relation links essentially the same cortical areas, but with a clear role of the parietal right cortical areas in the network of the primary motor areas.

In the case of the SCI population, the source and the target cortical patterns have a large size than in the normal population. The source cortical areas include always the primary motor areas of the foot as well as of the lips, often bilaterally. In addition, the right parietal and the bilateral area 6 are also present. The patterns remain substantially unchanged across the different frequency bands analyzed. The target cortical patterns observed in the SCI population have a larger extension when compared to the normal one, since they involving often the primary foot movement area as well as the SMA bilaterally. In addition, the presence of the bilateral primary lip area is also noted, in conjunction also with the participation of the bilateral parietal cortical areas.

A general pattern observed in both the populations analyzed is the reduction of the cortical areas involved in the network from the source patterns to the target patterns. In other words, we observed that a larger cortical network (the source) drives (or Granger-causes) the activity of a relative smaller set of cortical areas (the target). This was noted across all the frequency bands and all the subjects analyzed. However, due to the differences in the size of the source networks observed between normal and SCI patients, the general reduction of the size of the network of the target areas is not identical. Nevertheless, this phenomenon is evident in Figs. 3–8 which present the source and the target cortical areas during the preparation of the movement. A possible hypothesis is that, as the preparation for the action advances, there is a general reduction of the cortical areas that will be really involved in the final phase of the movement generation, from a preliminary phase in which a larger network has been engaged for the preparation of the joint movement. In general, the cortical networks involved in the SCI population are larger than those involved in the normal population, and this could be explained in the light of the impairment of the sensory-motor signal flows present in the SCI patients.

Conclusions

On the basis of the results obtained from the application of the described techniques to the movement preparation data, we were able to give the following answers to the questions posed in the ''Introduction'' section:

(1) There exist different cortical networks, elicited by the proposed volitional tasks, which are driving each other in the normal subjects as compared to the SCI patients.
(2). There are no specific frequency bands in which such causality relation between the cortical networks is maximally present during the investigated task. Rather, the relations between source and target cortical networks appear to be independent from the frequency band analyzed.
(3). There are significant differences in the cortical networks between normal subjects and SCI patients elicited during the investigated task. There is an increase in the size of the cortical network supporting the will to move in the SCI patients when compared to the normal population. It should be also noted that there is a general reduction of the size of the cortical networks in the causal transition from source to target, in both populations and for all the frequency bands analyzed.

The existence of such networks was already underlined in literature for simple movements in humans (reviewed in [43]). However, the class of movements investigated here has been chosen because their spatial details were known in advance, thus reducing the uncertainty about the possible results, which could be expected. In that way, we were able to test better the proposed methodology that combined independent component analysis and functional connectivity estimates. This combination of previously proven methods promises to help enhance the understanding of the properties of the brain cortical activity during motor and cognitive tasks in humans.

Acknowledgment This work was supported by a grant of RIKEN Institute for the years 2005–2007

Appendix

Estimation of functional connectivity by PDC

Let Y be a set of cortical waveforms, obtained from several cortical regions of interest (ROI):

$$\mathrm{Y}(t) = [\ y_1(t),\ y_2(t), \ldots, y_N(t)\ ]^{\mathrm{T}} \qquad (A.1)$$

where t refers to time and N is the number of cortical areas considered.

Supposing that the following MVAR process is an adequate description of the data set Y:

$$\sum_{k=0}^{p} \mathit{\Lambda}(k)\Upsilon(t-k) = \mathrm{E}(t) \qquad \text{with } \mathit{\Lambda}(0) = \mathbf{I} \tag{A.2}$$

where Y(t) is the data vector in time, $\mathbf{E}(t) = (e_1(t),..., e_N)^{\mathrm{T}}$ is a vector of multivariate zero-mean uncorrelated white noise processes, Λ(1), Λ(2) ... Λ(p) are the $N \times N$ matrices of model coefficients and p is the model order. In the present study, p was chosen by means of the Akaike Information Criteria (AIC) for MVAR processes [1] and was used for MVAR model fitting to simulations, as well as to experimental signals. It has been noted that, although the sensitivity of MVAR performance depends on the model order, small model order changes do not influence results [8, 22].

A modified procedure for the fitting of MVAR on multiple trials was adopted [3, 8, 21]. When many realizations of the same stochastic process are available, as in the case of several trials of an event-related potential (ERP) recording, the information from all the trials can be used to increase the reliability and statistical significance of the model parameters. In the present study, both in the simulation and in the application to real data, the data were in the form of several trials of the same length, as described in detail in the following sections.

Once an MVAR model is adequately estimated, it becomes the basis for subsequent spectral analysis. To investigate the spectral properties of the examined process, Eq. (2) is transformed to the frequency domain:

$$\mathit{\Lambda}(f)\ Y(f) = E(f) \tag{A.3}$$

where:

$$\mathit{\Lambda}(f) = \sum_{k=0}^{p} \mathit{\Lambda}(k)\ e^{-j2\pi f \Delta t k} \tag{A.4}$$

and Δt is the temporal interval between two samples.

Equation (3) can be rewritten as:

$$Y(f) = \mathit{\Lambda}^{-1}(f)\ E(f) = H(f)\ E(f) \tag{A.5}$$

H(f) is the transfer matrix of the system, whose element H_{ij} represents the connection between the jth input and the ith output of the system.

Baccalà and Sameshita [11] define the Partial Directed Coherence as:

$$\pi_{ij}(f) = \frac{\mathit{\Lambda}_{ij}(f)}{\sqrt{\sum_{k=1}^{N} \mathit{\Lambda}_{ki}(f)\mathit{\Lambda}_{kj}^{*}(f)}} \tag{A.6}$$

In this study, the squared version of PDC (sPDC) was used [4]:

$$\theta_{ij}(f) = \frac{\left|\mathit{\Lambda}_{ij}(f)\right|^2}{\sum_{m=1}^{N} \left|\mathit{\Lambda}_{mj}(f)\right|^2} \tag{A.7}$$

The θ_{ij}(f), describes the directional flow of information from the activity in the ROI $y_j(n)$ to the activity in $y_i(n)$, whereupon common effects produced by other ROIs $y_k(n)$ on the latter are subtracted, leaving only a description that is specifically from $y_j(n)$ to $y_i(n)$.

sPDC values are in the interval (0, 1), and the normalization condition

$$\sum_{n=1}^{N} \theta_{ni}(f) = 1 \tag{A.8}$$

is verified. According to this condition, $\theta_{ij}(f)$ represents the fraction of the time evolution of ROI j directed to ROI i, compared to all of j's interactions with other ROIs.

For PDC, high values in a frequency band represent the existence of an influence between any given pair of areas in the data set.

Independent component analysis and the ThinICA algorithm

Independent Component Analysis is a process which can extracts a new set of statistically independent components represented by the n-dimensional vector $\mathbf{y}(t) = \mathbf{W}\ \mathbf{x}(t)$ from exploratory (observed) input data represented by the m-dimensional vector $\mathbf{x}(t)$ (t = 1,2,...,N). The extracted components correspond to estimates of hidden or latent variables in the data called sometimes sources. This process assumes that a time series $\mathbf{x}(t)$ has an embedded mixing process of the form $\mathbf{x}(t) = \mathbf{A}\ \mathbf{s}(t)$, where $\mathbf{A}$ denotes an unknown mixing matrix and $\mathbf{s}(t)$ is a vector representing unknown hidden (latent) variables or sources. ICA can be considered as a demixing or a decomposition process which is able to recover the original sources, i.e., $\mathbf{y}(t) = \mathbf{s}(t)$, through the linear transformation $\mathbf{y}(t) = \mathbf{W}\ \mathbf{x}(t)$. The fact that two random variables are uncorrelated does not also imply that they are independent. This fact is lost in using other methods such as Principal Component Analysis (PCA). The ICA approach seeks to

find such independent directions through maximization of a suitable cost function called sometimes contrast function, which is a measure of statistical independence. Such functions can be maximized or minimized using various optimization methods, including artificial neural networks.

Independent component analysis can be considered as an extension of PCA. In PCA, the input data $\mathbf{x}(t)$ is decorrelated to find the components that are maximally uncorrelated according to second-order statistics. PCA gives orthogonalized and normalized outputs according to the second-order statistics by minimizing the second-order moments. The principal components can still be dependent however. The problem of ICA or blind source separation of sources mixed instantaneously can be defined as follows. Let's assume that we have available to us a set of multivariate time series $\{x_i(t)\}$ $(i = 1, 2, \ldots, m)$. We assume also that these time series, for example corresponding to individual EEG electrodes, are the result of an unknown mixing process defined by

$$x_i(t) = \sum_{j=1}^{n} a_{ij} s_j(t) \quad (i = 1, 2, \ldots, m) \tag{A.9}$$

or equivalently in compact matrix form $\{x_i(t)\}$ $(i = 1, 2, ..., m)$, where $\mathbf{A}$ is an unknown mixing matrix sized m by n, and $\mathbf{s}(t) = [s_1(t), s_2(t), \ldots, s_n(t)]^{\mathrm{T}}$ are hidden (latent) components called the sources. We seek to estimate the unknown sources $s_j(t)$ using only the observed data vector$\mathbf{x}(t) = [x_1(t), x_2(t), \ldots, x_m(t)]^{\mathrm{T}}$. The problem is to find a *demixing or separating matrix* $\mathbf{W}$ such that $\mathbf{y}(t) = \mathbf{W}\,\mathbf{x}(t)$ estimates the hidden independent components. It is possible that there could be a different numbers of sensors than sources, that is, $\mathbf{A}$ may not be square. If it is assumed that the number of sources (hidden components) is the same as the number of time series or observed inputs n, then $\mathbf{A}$ is a square (n by n) matrix. If $\mathbf{W} = \mathbf{A}^{-1}$, then $\mathbf{y}(t) = \mathbf{s}(t)$, and perfect separation occurs.

In practice, the optimal $\mathbf{y}$ will be some permutated and scaled version of $\mathbf{s}$, since it is only possible to find $\mathbf{W}$ such that $\mathbf{WA} = \mathbf{PD}$ where $\mathbf{P}$ is a permutation matrix and $\mathbf{D}$ is a diagonal scaling matrix. In general, the ICA of a random vector $\mathbf{x}(t)$ is obtained by finding a n by m, (with $m \geq n$), full rank separating (transformation) matrix $\mathbf{W}$ such that the output signal vector $\mathbf{y}(t) = [y_1(t), y_2(t), \ldots, y_n(t)]^{\mathrm{T}}$ (independent components) estimated by $\mathbf{y}(t) = \mathbf{W}\,\mathbf{x}(t)$, are as independent as possible.

Compared with the PCA, which removes second-order correlations from observed signals, ICA further removes higher-order dependencies. Statistical independence of random variables is a more general concept than decorrelation. Overall, we can state that random variables $y_i(t)$ and $y_i(t)$ are statistically independent if knowledge of the values of $y_i(t)$ provides no information about the values of $y_i(t)$. Mathematically, mutually independence of m random variables $y_j(t)$, $i = 1, \ldots, m$ can be expressed by $p(y) = p(y_1, \ldots, y_m) = \prod_{i=1}^{m} p(y_i)$, where $p(\mathbf{y})$ denotes the joint probability density function (pdf) of the random variable $\boldsymbol{y}(t)$. In other words, signals are independent if their joint pdf can be factorized into marginal distributions.

Second-order algorithms are not able to extract or separate random components without temporal structures such as i.i.d. (independent identically distributed) components. Therefore, in this study we used the ThinICA (or Thin SVD ICA) algorithm developed by Cruces and Cichocki [18]. The ThinICA algorithm can be considered as an extension of lower-order algorithms since it employs the second-order and higher-order statistics for the estimation of the rotation matrix $\mathbf{U}$ and, consequently, of the demixing matrix $\mathbf{W} = \hat{\mathbf{A}}^{-1} = \mathbf{U}^{\mathrm{T}}\mathbf{Q}$. The ThinICA algorithm is able to extract simultaneously arbitrary number of components specified by the user. The algorithm is based on a criterion that jointly performs the maximization of several third- and/or fourth-order cumulants of the outputs and/or second-order time-delayed covariance matrices, i.e., on the maximization of the following contrast function:

$$J(\mathbf{U}) = \sum_{i=1}^{n} \sum_{\tau} \alpha_\tau [Cum(y_i(t_1), y_i(t_2), \ldots, y_i(t_P))]^2 \tag{A.10}$$

subject to the constraints $\mathbf{U}^{\mathrm{T}}\,\mathbf{U} = I_{\mathrm{n}}$, where α_τ are weighting coefficients (typically, equal to 1) and *Cum* means cumulants for different time tuples $\tau = \{t_1, t_2, \ldots, t_P\}$. In practice, we have used only the 2nd, 3rd and 4th order cumulants [16, 18].

The contrast function employed for ThinICA combines the robustness of the joint approximate diagonalization techniques with the flexibility of the methods for blind signal extraction. Its maximization leads to hierarchical and simultaneous ICA extraction algorithms which are based on the thin SVD factorizations. The practical implementation of the ThinICA algorithm is available on the following web page: http://www.bsp.brain.riken.jp/ICALAB/.

After extracting the independent components or performing blind separation of signals (from the mixture), we can examine the effects of discarding some non-significant components by reconstructing the observed EEG data from the remaining components. This procedure is called deflation or reconstruction, and allows us to remove unnecessary (or undesirable) components that are hidden in the mixture (superimposed or overlapped EEG data). The deflation algorithm eliminates one or more components from the vector $\boldsymbol{y}(t)$ and then performs the back-propagation

$\mathbf{X_r} = \mathbf{W}^*\mathbf{Y_r}$, where $\mathbf{X}_r(t)$ is a vector of reconstructed input (exploratory) data $\mathbf{X}(t)$, $\mathbf{W}^* = \hat{\mathbf{A}}$ is a generalized pseudo inverse matrix of the estimated demixing matrix $\mathbf{W}$, and $\mathbf{y}_r(t)$ is the vector obtained from the vector of independent components $\boldsymbol{y}(t)$ after removal of all the undesirable components (i.e., by replacing them with zeros).

ICA is a process which statistically reduces a possibly very multidimensional complex data set into sub-components which are statistically independent, and which are expected to capture most of the useful information regarding the underlying events. Since properly estimated ICs are statistically independent from each other, they can be used to create a new set of explanatory variables in order to investigate brain signal relationships more efficiently than it would be possible with the unprocessed data, and can be used by exploratory techniques like DTF or PDC.

Estimation of Cortical Source Current Density

The solution of the following linear system:

$$\mathbf{A_L}\,\mathbf{x} = \mathbf{b} + \mathbf{n} \tag{A.11}$$

provides an estimation of the dipole source configuration $\mathbf{x}$ that generates the measured EEG potential distribution $\mathbf{b}$. The system includes also the measurement noise $\mathbf{n}$, assumed to be normally distributed. $\mathbf{A_L}$ is the lead field matrix, where each jth column describes the potential distribution generated on the scalp electrodes by the jth unitary dipole. The current density solution vector ξ of A.4 was obtained as [27]:

$$\xi = \arg\min_{x}\left(\|\mathbf{A}_L\mathbf{x} - \mathbf{b}\|^2_{\mathbf{M}} + \lambda^2\|\mathbf{x}\|^2_{\mathbf{N}}\right) \tag{A.12}$$

where $\mathbf{M}$, $\mathbf{N}$ are the matrices associated to the metrics of the data and of the source space, respectively, λ is the regularization parameter and $\| \mathrm{x} \|_{\mathrm{M}}$ represents the M norm of the vector $\mathbf{x}$. The solution of A.5 is given by the inverse operator G:

$$\xi = \mathbf{Gb}, \quad \mathbf{G} = \mathbf{N}^{-1}\mathbf{A}\prime_{\mathbf{L}}\left(\mathbf{A_L}\mathbf{N}^{-1}\mathbf{A}'_{\mathrm{L}} + \lambda\mathbf{M}^{-1}\right)^{-1} \tag{A.13}$$

An optimal regularization of this linear system was obtained by the L-curve approach [30, 31]. As a metric in the data space we used the identity matrix, while as a norm in the source space we use the following metric:

$$(\mathbf{N}^{-1})_{ii} = \|\mathbf{A}_{\cdot i}\|^{-2} \tag{A.14}$$

where $(\mathbf{N}^{-1})_{ii}$ is the ith element of the inverse of the diagonal matrix $\mathbf{N}$ and all the other matrix elements N_{ij} are set to 0. The L_2 norm of the ith column of the lead field matrix $\mathbf{A}$ is denoted by $\|\mathbf{A_i}\|$.

Estimated cortical waveforms

Using the relations described above, an estimate of the signed magnitude of the dipolar moment for each one of the 5000 cortical dipoles was obtained for each time point. As the orientation of the dipole was defined to be perpendicular to the local cortical surface in the head model, the estimation process returned a scalar rather than a vector field. To obtain the cortical current waveforms for all the time points, we used a unique ''quasi-optimal'' regularization λ value for all the analyzed EEG potential distributions. The quasi-optimal regularization value was computed as an average of the several λ values obtained by solving the linear inverse problem for a series of EEG potential distributions. These distributions are characterized by an average Global Field Power (GFP) with respect to the higher and lower GFP values obtained from all the recorded waveforms. The instantaneous average of the signed magnitude of all the dipoles belonging to a particular ROI was used to estimate the average cortical activity in that ROI, during the entire interval of the experimental task. These waveforms were then subjected to the MVAR estimation, in order to estimate the connectivity pattern between ROIs. For a given ROI pair, the significance of the estimated cortical connectivity pattern was determined by comparison of its value to a threshold level. To estimate the thresholds for the functions values indicating lack of transmission, a surrogate data generation procedure was performed [3]. The time series data from each ROI were randomly shuffled in order to remove interactions between signals. The connectivity estimators were then computed on these surrogate data. The procedure was repeated 1,000 times, and an empirical distribution was generated. The significance threshold was set at 0.01. Only values beyond this threshold were considered to indicate the existence of a connection between each pair of ROIs.

References

1. Akaike H. A new look at statistical model identification. IEEE Trans Automat Control AC, 1974;19:716–23.
2. Astolfi L, Cincotti F, Babiloni C, Carducci F, Basilisco A, Rossini PM, Salinari S, Mattia D, Cerutti S, Ben Dayan D, Ding L, Ni Y, He B, Babiloni F Estimation of the cortical connectivity by high resolution EEG and structural equation modeling: simulations and application to finger tapping data. IEEE Trans Biomed Eng 2005a;52(5):757–68.
3. Astolfi L, Cincotti F, Mattia D, Babiloni C, Carducci F, Basilisco A, Rossini PM, Salinari S, Ding L, Ni Y, He B, Babiloni F. Assessing cortical functional connectivity by linear inverse estimation and directed transfer function: simulations and application to real data. Clin Neurophysiol 2005b;116(4):920–32.
4. Astolfi L, Cincotti F, Mattia D, Marciani MG, Baccala LA, de Vico Fallani F, Salinari S, Ursino M, Zavaglia M, Babiloni F.

Assessing cortical functional connectivity by partial directed coherence: simulations and application to real data. IEEE Trans Biomed Eng 2006;53(9):1802–12.
5. Babiloni F, Babiloni C, Carducci F, Romani GL, Rossini PM, Angelone LM, Cincotti F. Multimodal integration of EEG and MEG data: a simulation study with variable signal-to-noise ratio and number of sensors. Hum Brain Mapp 2004;22(1):52–62.
6. Babiloni F, Babiloni C, Carducci F, Romani GL, Rossini PM, Angelone LM, Cincotti F. Multimodal integration of high-resolution EEG and functional magnetic resonance imaging data: a simulation study. Neuroimage 2003;19(1):1–15.
7. Babiloni F, Babiloni C, Locche L, Cincotti F, Rossini PM, Carducci F. High-resolution electroencephalogram: source estimates of Laplacian-transformed somatosensory-evoked potentials using a realistic subject head model constructed from magnetic resonance images. Med Biol Eng Comput 2000;38(5):512–9.
8. Babiloni F, Cincotti F, Babiloni C, Carducci F, Basilisco A, Rossini PM, Mattia D, Astolfi L, Ding L, Ni Y, Cheng K, Christine K, Sweeney J, He B. Estimation of the cortical functional connectivity with the multimodal integration of high resolution EEG and fMRI data by Directed Transfer Function. Neuroimage 2005;24(1):118–31.
9. Babiloni F, Carducci F, Cincotti F, Del Gratta C, Pizzella V, Romani GL, Rossini PM, Tecchio F, Babiloni C. Linear inverse source estimate of combined EEG and MEG data related to voluntary movements. Human Brain Mapp 2001;14(3).
10. Baccalà LA. On the efficient computation of partial coherence from multivariate autoregressive model. In: Callaos N, Rosario D, Sanches B editors. Proceedings of the 5th world conference cybernect is systemics and informatics SCI 2001, Orlando; 2001.
11. Baccalà LA, Sameshima K. Partial directed coherence: a new concept in neural structure determination. Biol Cybern 2001;84:463–74.
12. Bakardjian H. Common independent components for motion-based brain-computer-interfaces. In: Proc. of the society for NeuroScience meeting, San Diego, USA, Oct 23–27; 2004.
13. Brovelli A, Battaglini PP, Naranjo JR, Budai R. Medium-range oscillatory network and the 20-Hz sensorimotor induced potential. Neuroimage 2002;16(1):130–41.
14. Brovelli A, Ding M, Ledberg A, Chen Y, Nakamura R, Bressler SL. Beta oscillations in a large-scale sensorimotor cortical network: directional influences revealed by Granger causality. Proc Natl Acad Sci USA 2004;101(26):9849–54.
15. Buchel C, Friston KJ (1997) Modulation of connectivity in visual pathways by attention: cortical interactions evaluated with structural equation modeling and fMRI. Cereb Cortex 7(8):768–78.
16. Cichocki A, Amari S. Adaptive blind signal and image processing: learning algorithms and applications. West Sussex, UK: John Wiley & Sons; 2003.
17. Clifford Carter G. Coherence and time delay estimation. Proc IEEE 1987;75:236–55.
18. Cruces-Alvarez S, Cichocki A. Combining blind source extraction with joint approximate diagonalization: thin algorithms for ICA. In: Proceedings of 4th international symposium on independent component analysis and blind signal separation (ICA2003), Kyoto, Japan, Riken, ICA; Apr., 2003, p. 463–8.
19. Cruces-Alvarez S, Cichocki A, De Lathauwer L. Thin QR and SVD factorizations for simultaneous blind signal extraction. In: Proceedings of the European Signal Processing Conference (EUSIPCO), Vienna, Austria; 2004, p. 217–220, ISBN: 3-200-00165-8.
20. David O, Cosmelli D, Friston KJ. Evaluation of different measures of functional connectivity using a neural mass model. Neuroimage 2004;21(2):659–73.
21. Ding M, Bressler SL, Yang W, Liang H. Short-window spectral analysis of cortical event related potentials by adaptive multivariate autoregressive modeling: data preprocessing, model validation and variability assessment. Biol Cybern 2000;83:35–45.
22. Franaszczuk PJ, Blinowska KJ, Kowalczyk M. The application of parametric multichannel spectral estimates in the study of electrical brain activity. Biol Cybern 1985;51:239–47.
23. Friston KJ. Functional and effective connectivity in neuroimaging: a synthesis. Human Brain Mapp 1994;2:56–78.
24. Gerloff C, Richard J, Hadley J, Schulman AE, Honda M, Hallett M. Functional coupling and regional activation of human cortical motor areas during simple, internally paced and externally paced finger movements. Brain 1998;121(Pt 8):1513–31.
25. Gevins AS, Cutillo BA, Bressler SL, Morgan NH, White RM, Illes J, Greer DS. Event-related covariances during a bimanual visuomotor task. II. Preparation and feedback. Electroencephalogr Clin Neurophysiol 1989;74:147–60.
26. Granger CWJ. Investigating causal relations by econometric models and cross-spectral methods. Econometrica 1969;37:424–38.
27. Grave de Peralta Menendez R, Gonzalez Andino SL. Distributed source models: standard solutions and new developments. In: Uhl C, editor. Analysis of neurophysiological brain functioning. Springer Verlag; 1999. p. 176–201.
28. Gross J, Kujala J, Hämäläinen M, Timmermann L, Schnitzler A, Salmelin R. Dynamic imaging of coherent sources: studying neural interactions in the human brain. Proc Natl Acad Sci USA 2001;98(2):694–99.
29. Gross J, Timmermann L, Kujala J, Salmelin R, Schnitzler A. Properties of MEG tomographic maps obtained with spatial filtering. NeuroImage 2003;19:1329–36.
30. Hansen PC. Analysis of discrete ill-posed problems by means of the L-curve. SIAM Rev 1992a;34:561–80.
31. Hansen PC. Numerical tools for the analysis and solution of Fredholm integral equations of the first kind. Inverse Prob 1992b;8:849–72.
32. He B, Lian J. Spatio-temporal functional neuroimaging of brain electric activity. Crit Rev Biomed Eng 2002;30:283–306.
33. Horwitz B. The elusive concept of brain connectivity. Neuroimage 2003;19(2Pt1):466–70.
34. Inouye T, Iyama A, Shinosaki K, Toi S, Matsumoto Y. Inter-site EEG relationships before widespread epileptiform discharges. Int J Neurosci 1995;82:143–53.
35. Jancke L, Loose R, Lutz K, Specht K, Shah NJ. Cortical activations during paced finger-tapping applying visual and auditory pacing stimuli. Brain Res Cogn Brain Res 2000;10(1–2):51–66.
36. Kaminski M, Ding M, Truccolo WA, Bressler S. Evaluating causal relations in neural systems: Granger causality, directed transfer function and statistical assessment of significance. Biol Cybern 2001;85:145–57.
37. Korzeniewska A, Manczak M, Kaminski M, Blinowska K, Kasicki S. Determination of information flow direction between brain structures by a modified Directed Transfer Function method (dDTF). J Neurosci Methods 2003;125:195–207.
38. Lee L, Harrison LM, Mechelli A. The functional brain connectivity workshop: report and commentary. Neuroimage 2003;19:457–465.
39. Miwakeichi F, Martinez-Montes E, Valdes-Sosa PA, Nishiyama N, Mizuhara H, Yamaguchi Y. Decomposing EEG data into space-time-frequency components using parallel factor analysis. NeuroImage 2004;22:1035–45.
40. Mizuhara H, Wang L, Kobayashi K, Yamaguchi Y. Long-range EEG phase synchronization during an arithmetic task indexes a coherent cortical network simultaneously measured by fMRI. NeuroImage 2005;27(3):553–63.
41. Nunez PL. Neocortical dynamics and human EEG rhythms. Oxford University Press, New York; 1995.

42. Pascual-Marqui RD. Reply to comments by Hama lainen, Ilmoniemi and Nunez. In: Skrandies W, editor. ISBET Newsletter No. 6; December, 1995. p. 16–28.
43. Pfurtscheller G, Lopes da Silva FH. Event-related EEG/MEG synchronization and desynchronization: basic principles. Clin Neurophysiol 1999;110(11):1842–57.
44. Picard N, Strick PL. Imaging the premotor areas. Curr Opin Neurobiol 1996;11(6):663–72.
45. Pollok B, Gross J, Muller K, Aschersleben G, Schnitzler A. The cerebral oscillatory network associated with auditorily paced finger movements. NeuroImage 2005a;24:646–55.
46. Pollok B, Gross J, Muller K, Aschersleben G, Schnitzler A. The oscillatory network of simple repetitive bimanual movements. Cogn Brain Res 2005b;25:300–11.
47. Quian Quiroga R, Kraskov A, Kreuz T, Grassberger P. Performance of different synchronization measures in real data: a case study on electroencephalographic signals. Phys Rev;2002 E 65p., 041903.
48. Rosenblum MG, Pikovsky AS. Detecting direction of coupling in interacting oscillators. Phys Rev, E Stat. Nonlinear Soft Matter Phys 2001;64:045202.
49. Stam CJ, Breakspear M, van Cappellen, van Walsum AM, van Dijk BW. Nonlinear synchronization in EEG and whole head MEG recordings of healthy subjects. Hum Brain Mapp 2003;19(2):63–78.
50. Stam CJ, van Dijk BW. Synchronization likelihood: an unbiased measure of generalized synchronization in multivariate data sets. Physica D 2002;163: 236–51.
51. Taniguchi M, Kato A, Fujita N, Hirata M, Tanaka H, Kihara T, Ninomiya H, Hirabuki N, Nakamura H, Robinson SE, Cheyne D, Yoshimine T. Movement-related desynchronization of the cerebral cortex studied with spatially filtered magnetoencephalography. Neuroimage 2000;12(3):298–306.
52. Tononi G, Sporns O, Edelman GM. A measure for brain complexity: relating functional segregation and integration in the nervous system. Proc Natl Acad Sci USA 1994;91: 5033–7.
53. Urbano A, Babiloni C, Onorati P, Babiloni F. Dynamic functional coupling of high resolution EEG potentials related to unilateral internally triggered one-digit movements. Electroencephalogr Clin Neurophysiol 1998;106(6):477–87.